23rd ABCM International Congress of Mechanical Engineering
December 6-11, 2015, Rio de Janeiro, RJ, Brazil

NONLINEAR INVESTIGATION OF CHAOS AND HYPERCHAOS IN A 2-DOF SHAPE MEMORY OSCILLATOR

Guilherme Vieira Rodrigues
Alberto Paiva
Larissa Maciel da Fonseca

Universidade Federal Fluminense
Volta Redonda School of Engineering
Department of Mechanical Engineering
420 Trabalhadores Av.
Volta Redonda – RJ – Brazil – 27.255-250
guilherme_@live.co.uk; paiva.ufrj@gmail.com (corresponding author); larissamaciel.lah@gmail.com

Abstract. *The increasing interest in smart structures applications has been motivating the study of dynamical systems incorporating the so-called intelligent materials. The hysteretic behavior inherent to such materials turns their respective formulation intrinsically nonlinear, enabling plentiful dynamical responses, ranging from periodic to chaotic solutions. This paper aims to explore the chaos occurrence and their consequences in a two-degree of freedom sketch with shape memory alloy (**SMA**) restoring elements. The constitutive modeling of **SMA** considers a polynomial first-order phase transition formulation, which may be included in the dynamical model. The resulting set of coupled ordinary differential equations is solved using a fourth-order Runge-Kutta scheme. Numerical results take into account specific nonlinear phenomena such as: crisis, chaos and hyperchaos.*

Keywords: *Shape memory alloy, nonlinear dynamics, chaos, hyperchaos.*

1. INTRODUCTION

Shape Memory Alloy (**SMA**) systems and structures applications have become popularized in the last two decades, not only due to **SMA**'s outstanding capacity to develop and recover high strain levels (or to develop huge restoring forces, while constraining their displacement) but also because of their intrinsic damping capacity, both deriving from hysteretic reversible phase transformations. These features enable an adaptive behavior inherent to **SMA** devices (a.k.a. intelligent structures), which motivates their use as sensors and, especially, as actuators. Within this context, static (quasi-static) and dynamical applications may be found in the literature, concerning different fields, such as: naval, aeronautical, aerospace, automotive, civil, automation and control, oil and gas, among other non-engineering fields, just like medical and dental industries. Among static and quasi-static applications, there are: compressive clamps; robotic claws; position actuators; self-expanding washers; airfoils, hydrofoils and adaptive wings (morphing). Among dynamical applications, there are: undersea and in-land robots, micro and nano-electromechanical systems (MEMS and NEMS, respectively) and adaptive bearings to control vibrations in rotating machines. For more details about **SMA** applications, please refer to the following references: Wayman (1980); Duerig *et al*. (1990); Birman (1997); Otsuka & Wayman (1998); Paiva and Savi (2006); Lagoudas (2008), among others.

A substantial number of articles concerning nonlinear dynamical analysis of mechanical systems using **SMA** may be found in the literature, such as the following articles. Williams *et al*. (2002) design an adaptive-passive absorber using **SMA** wires to attenuate mechanical vibrations in an experimental prototype. Lagoudas *et al*. (2004) explore the **SMA** damping capacity to develop a numerical-experimental analysis of a pseudoelastic spring used for passive vibration isolation. Seelecke (2002) explores the effect of change in temperature of the **SMA** element under torsional mechanical vibration due to the fact that there is not enough time to perform the necessary latent heat exchange. Bernardini & Rega (2005) also evaluated the influence of loading rate dependence of the constitutive model over the dynamical response of a **SMA** oscillator. Savi and co-workers have developed dynamical analyses of different **SMA** mechanical systems. In the following works: Savi & Pacheco (2002) and Machado *et al*. (2003, 2004), the authors investigate nonlinear features of one and two-degree of freedom oscillators using the same polynomial constitutive model used herein. Savi *et al*. (2008) use a more elaborate constitutive model with internal constraints to evaluate the influence of tension-compression asymmetry over the dynamical response of a one-degree of freedom **SMA** oscillator. Santos & Savi (2009) examine the nonlinear dynamics of a nonsmooth one-degree of freedom oscillator with a discontinuous **SMA** support. Savi *et al*. (2011) design an adaptive vibration absorber using a **SMA** coupling element. Silva *et al*. (2013) numerically simulate the nonlinear behavior of a two-degree of freedom *Jeffcot* rotor with **SMA** restoring elements on bearings.

While modeling most of nowadays applications, simple mechanical sketches may provide suitable solutions for practical purposes. Nevertheless, when the **SMA** behavior is incorporated to even simple physical models, the resulting mathematical formulation is highly nonlinear – especially in time-varying problems, unveiling all the dynamical richness of this kind of system. Thus, for a successful designing, a thorough comprehension of the smart structure dynamical response is something imperative. With this goal, this work deals with the mechanical modeling and numerical simulation of a two-degree of freedom oscillator using three **SMA** restoring elements. The **SMA** constitutive behavior is described through a polynomial first-order phase transition formulation, originally proposed by Falk (1980). The resulting set of coupled ordinary differential equations is solved using a fourth-order Runge-Kutta scheme. Numerical results for a damped harmonically forced system consider trajectories on state subspaces and *Poincare* sections for different qualitative behaviors ranging from periodic to chaotic/hyperchaotic solutions, based on a bifurcation diagram varying the temperature of the intermediate **SMA** element. At last, *Lyapunov* exponents are used not only to attest periodic responses but also to distinguish chaos from hyperchaos.

2. MATHEMATICAL MODELING

This section comprises the dynamical physical model and its respective mathematical formulation, incorporating the **SMA** polynomial constitutive model. Aiming an optimized numerical implementation, the resulting set of ordinary differential equations of motion is put in a dimensionless form. At last, the numerical procedures are discussed.

Figure 1 presents the physical model for a two-degree of freedom oscillator with **SMA** restoring elements, where: m_1 and m_1 are lumped masses with linear displacements along 'x" direction denoted by $u_1(t)$ and $u_2(t)$, respectively; c_1, c_2 and c_3 are damping coefficients; $F_1(t)$ and $F_2(t)$ are external harmonic excitations and $K_1(u)$, $K_2(u)$ and $K_3(u)$, are nonlinear stiffness associated with the **SMA** elements.

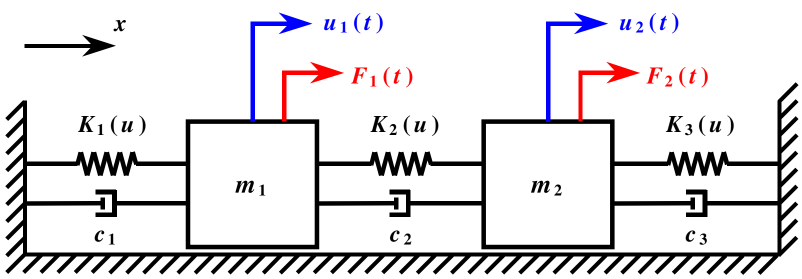

Figure 1. Two-degree of freedom **SMA** oscillator physical model.

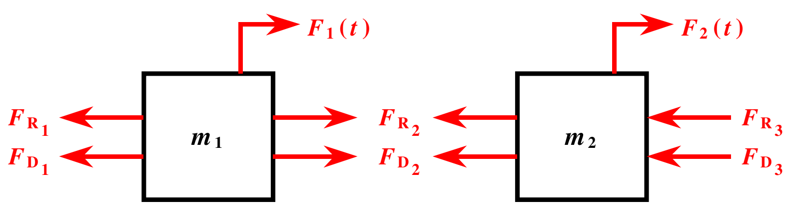

Figure 2. Free-body diagram for **SMA** oscillator.

According to the free-body diagram presented in Fig. 2, Newton's equations of motion for each mass provide:

$$\begin{cases} -F_{R_1} - F_{D_1} + F_{R_2} + F_{D_2} + F_1(t) = m_1 \ddot{u}_1 & \Rightarrow \text{ for mass } m_1 \\ -F_{R_2} - F_{D_2} - F_{R_3} - F_{D_3} + F_2(t) = m_2 \ddot{u}_2 & \Rightarrow \text{ for mass } m_2 \end{cases} \tag{1}$$

The polynomial constitutive stress-strain relation proposed by Falk (1980) to describe **SMA** behavior is given by:

$$\sigma = a\,(T - T_M)\,\varepsilon - b\,\varepsilon^3 + e\,\varepsilon^5 \tag{2}$$

where: a, b and $e = b^2 / 4a\,(T_A - T_M)$ are material parameters; σ and ε are the uniaxial stress and strain, respectively; T is the absolute temperature, whereas T_A and T_M are the beginning transformation temperatures for austenite and martensite formation, respectively.

The restoring forces F_{R_i} (for i = 1,2,3) acting on the **SMA** elements may be considered as $F_{R_i} = A\,\sigma_i$, while the uniaxial strain may be assumed as: $\varepsilon_i = \Delta u_i \,/\, L$. The parameters A and L are the cross-sectional area and the length of the **SMA** elements (assumed the same for all of them) and Δu_i represents the elongation of each **SMA** element. Considering all three elements with the same material parameters, the restoring forces F_{R_i} are defined as follows:

$$F_{R_i} = \left[a\left(T_i - T_M\right)\frac{\Delta u_i}{L} - b\left(\frac{\Delta u_i}{L}\right)^3 + e\left(\frac{\Delta u_i}{L}\right)^5 \right] A \qquad \text{(for } i = 1,2,3\text{)} \tag{3}$$

Moreover, linear dissipation forces for F_{D_i} are considered, while $F_j\left(t\right) = f_j \sin\left(\Omega_j\, t\right)$ where f_j are the forcing amplitudes and Ω_j the forcing angular frequencies (for j = 1,2). Substitution of the expressions specified for: F_{R_i}, F_{D_i} (i = 1,2,3) and $F_j\left(t\right)$ (j = 1,2) in Eq. (1), leads to:

$$\begin{cases} m_1 L^5\, \ddot{u}_1 + \left(c_1 + c_2\right) L^5\, \dot{u}_1 - c_2 L^5\, \dot{u}_2 + a\,A\,L^4 \left[\left(T_1 - T_M\right) u_1 - \left(T_2 - T_M\right)\left(u_2 - u_1\right)\right] - \\ \qquad - b\,A\,L^2 \left[u_1^3 - \left(u_2 - u_1\right)^3\right] + e\,A\left[u_1^5 - \left(u_2 - u_1\right)^5\right] = F_1 L^5 \sin\left(\Omega_1\, t\right) \\ m_2 L^5\, \ddot{u}_2 - c_2 L^5\, \dot{u}_1 + \left(c_2 + c_3\right) L^5\, \dot{u}_2 + a\,A\,L^4 \left[\left(T_2 - T_M\right)\left(u_2 - u_1\right) + \left(T_3 - T_M\right) u_2\right] - \\ \qquad - b\,A\,L^2 \left[\left(u_2 - u_1\right)^3 + u_2^3\right] + e\,A\left[\left(u_2 - u_1\right)^5 + u_2^5\right] = F_2 L^5 \sin\left(\Omega_2\, t\right) \end{cases} \tag{4}$$

To obtain the dimensionless differential equations of motion, consider the new variables: $\tau = \omega t$ as the new independent variable, where ω is an angular frequency concerning a reference value; while $U_1 = u_1 \big/ L$ and $U_2 = u_2 \big/ L$ are the new dimensionless displacements for the masses m_1 and m_2, respectively.

At this point, the original variables u_1 (t) and u_2 (t) and their derivatives are substitued for the new dimensionless variables U_1 (τ) and U_2 (τ), regarding that: $U_i = U_i\left(\tau\left(t\right)\right)$ (for j = 1,2). Therefore, by applying the chain's rule, $\dot{u}_i = L\,\omega\, U_i^{'}$ and $\ddot{u}_i = L\,\omega^2\, U_i^{''}$, where: $U_i^{'} = d\,U_i \big/ d\,\tau$. Moreover, the first of Eqs. (4) related to m_1 is simplified by the factor $m_1 L^5\,\omega^2$, while the second equation related to m_2 is simplified by the factor $m_2 L^5\,\omega^2$. After all these algebraic procedures, eventually, the following set of second-order ordinary differential equations arises:

$$\begin{cases} U_1^{''} + \alpha\, U_1^{'} - \beta\, U_2^{'} + \phi\left[\left(\theta_1 - 1\right) U_1 - \left(\theta_2 - 1\right)\left(U_2 - U_1\right)\right] - \gamma\left[U_1^3 - \left(U_2 - U_1\right)^3\right] + \\ \qquad + \eta\left[U_1^5 - \left(U_2 - U_1\right)^5\right] = \delta_1 \sin\left(\varpi_1\, \tau\right) \\ U_2^{''} - \xi\, U_1^{'} + \mu\, U_2^{'} + \rho\left[\left(\theta_2 - 1\right)\left(U_2 - U_1\right) + \left(\theta_3 - 1\right) U_2\right] - \varphi\left[\left(U_2 - U_1\right)^3 + U_2^3\right] + \\ \qquad + \lambda\left[\left(U_2 - U_1\right)^5 + U_2^5\right] = \delta_2 \sin\left(\varpi_2\, \tau\right) \end{cases} \tag{5}$$

Concerning the new dimensionless parameters, they are related to the original ones as follows:

$$\begin{array}{llllll} \alpha = \dfrac{c_1 + c_2}{m_1\,\omega}; & \beta = \dfrac{c_2}{m_1\,\omega}; & \phi = \dfrac{a\,A\,T_M}{m_1\,L\,\omega^2}; & \gamma = \dfrac{b\,A}{m_1\,L\,\omega^2}; & \eta = \dfrac{e\,A}{m_1\,L\,\omega^2}; & \delta_1 = \dfrac{F_1}{m_1\,L\,\omega^2} \\ \xi = \dfrac{c_2}{m_2\,\omega}; & \mu = \dfrac{c_2 + c_3}{m_2\,\omega}; & \rho = \dfrac{a\,A\,T_M}{m_2\,L\,\omega^2}; & \varphi = \dfrac{b\,A}{m_2\,L\,\omega^2}; & \lambda = \dfrac{e\,A}{m_2\,L\,\omega^2}; & \delta_2 = \dfrac{F_2}{m_2\,L\,\omega^2} \end{array} \tag{6}$$

In addition to that, consider the dimensionless forcing frequency $\varpi_j = \Omega_j / \omega$ (j = 1,2) and also the dimensionless temperature $\theta_i = T_i / T_M$ (i = 1,2,3). Assuming $m_1 = m_2 = 1$, results in: $\beta = \xi$; $\phi = \rho$; $\gamma = \varphi$; $\eta = \lambda$. Besides, if the reference angular frequency is defined as: $\omega = \sqrt{a\, A\, T_M / m_1\, L}$, thus $\phi = \rho = 1$.

For the purpose of numerical implementation via fourth-order Runge-Kutta method, it is necessary to convert the original system consisting of two second-order ordinary differential equations into a new set of first-order ordinary differential equations with four equations. Hence, consider a new variables' change, such that: $U_1 = x$; $U_1^{'} = y$; $U_2 = w$; $U_2^{'} = z$, where the new derivatives denoted by ($^\bullet$) correspond to $(\,^\bullet\,) = d(\;)/d\tau$. Finally, the dynamical governing differential equations in their ultimate form are given by:

$$\begin{cases} \dot{x} = y \\ \dot{y} = \delta_1 \sin(\varpi_1 \tau) - \alpha\, y + \beta\, z - [(\theta_1 - 1)\, x - (\theta_2 - 1)(w - x)] + \gamma\left[x^3 - (w - x)^3\right] - \eta\left[x^5 - (w - x)^5\right] \\ \dot{w} = z \\ \dot{z} = \delta_2 \sin(\varpi_2\, \tau) + \beta\, y - \mu\, z - [(\theta_2 - 1)(w - x) + (\theta_3 - 1)\, w] + \gamma\left[(w - x)^3 + w^3\right] - \eta\left[(w - x)^5 + w^5\right] \end{cases} \tag{7}$$

3. NUMERICAL RESULTS

This section shows the numerical results obtained for damped harmonically forced cases. Initially, several dynamical patterns are identified through a bifurcation diagram varying the temperature of the intermediate **SMA** element. Then, their respective trajectories and *Poincare* sections on state subspaces are presented. At last, *Lyapunov* exponents are evaluated to verify the different dynamical responses previous obtained. Both the dynamical system parameters and the **SMA** parameters used in all simulations along this paper are presented in Tabs. 1 and 2.

Figure 3 shows bifurcation diagrams for the dimensionless displacements U_1 and U_2, varying with the dimensionless temperature θ_2 of the intermediate **SMA** element, where three distinct chaotic-like regions are identified in both Figs. 3(a) and 3(b). Depicted in the first detail of each of the two figures (for 1.74 < θ_2 < 1.81), it is possible to identify a periodic window with period-1 immersed in the first chaotic-like region. Concerning the third chaotic-like region (for 2.25 < θ_2 < 2.6), two typical nonlinear phenomena are recognized, as follows: before this region, there is a bifurcation cascading towards chaos, as depicted in the second detail of each of the two figures and, after this region, for higher temperatures, the chaotic behavior suddenly becomes a period-1 response (for $\theta_2 \cong$ 2.6), characterizing what is known as crisis.

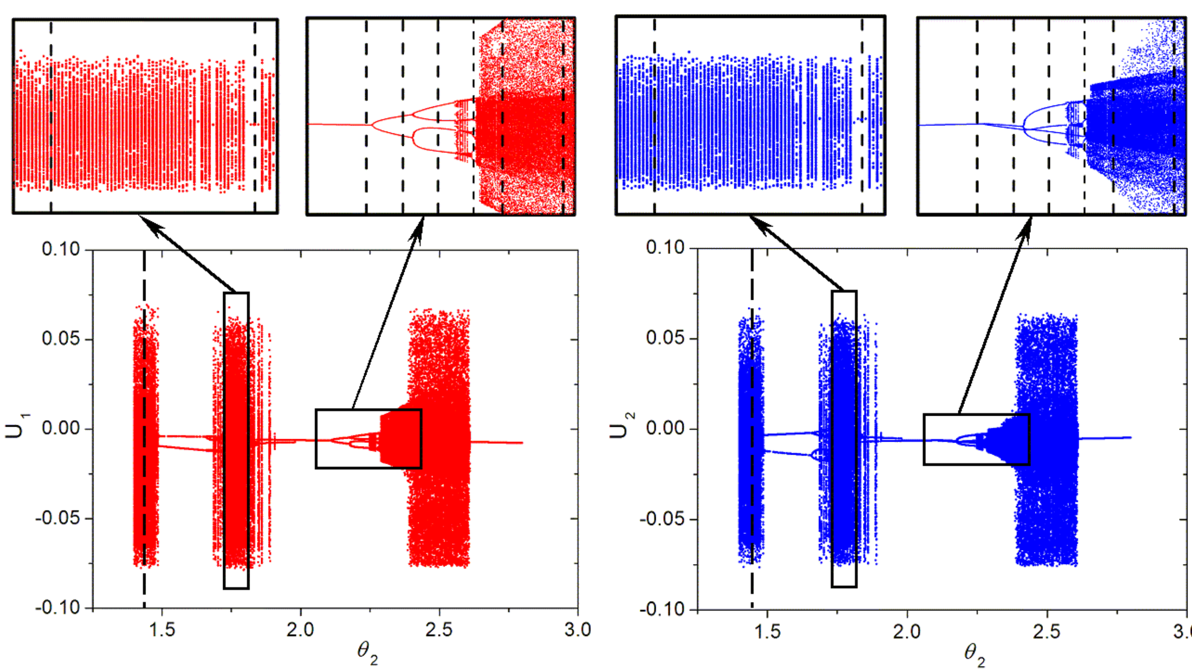

(a) (b)

Figure 3. Bifurcation diagrams varying the dimensionless temperature θ_2 of the intermediate **SMA** element. (a) U_1 x θ_2 ; (b) U_2 x θ_2 .

Table 1. Dynamical System Parameters.

$\alpha = \beta = \mu$	$\delta_1 = \delta_2$	$\varpi_1 = \varpi_2$
0.10	0.06	1.00

Table 2. **SMA** Parameters.

γ	η	θ_1	θ_3
1.30 x 10^3	4.70 x 10^5	1.00	1.50

Based on the bifurcation diagrams presented in Fig. 3, nine selected values of the dimensionless temperature θ_2 are selected (according to the dashed lines present in the main figures and in the depicted details) to illustrate different dynamical patterns (including periodic and chaotic-like situations).

Figures 4 and 5 show the respective trajectories on state subspaces U_1 x U_2 x U_1' and *Poincare* sections for the following conditions: $\theta_2 = 1.44$; $\theta_2 = 1.75$; $\theta_2 = 1.804$; $\theta_2 = 2.10$; $\theta_2 = 2.15$; $\theta_2 = 2.20$; $\theta_2 = 2.28$; $\theta_2 = 2.34$; $\theta_2 = 2.44$.

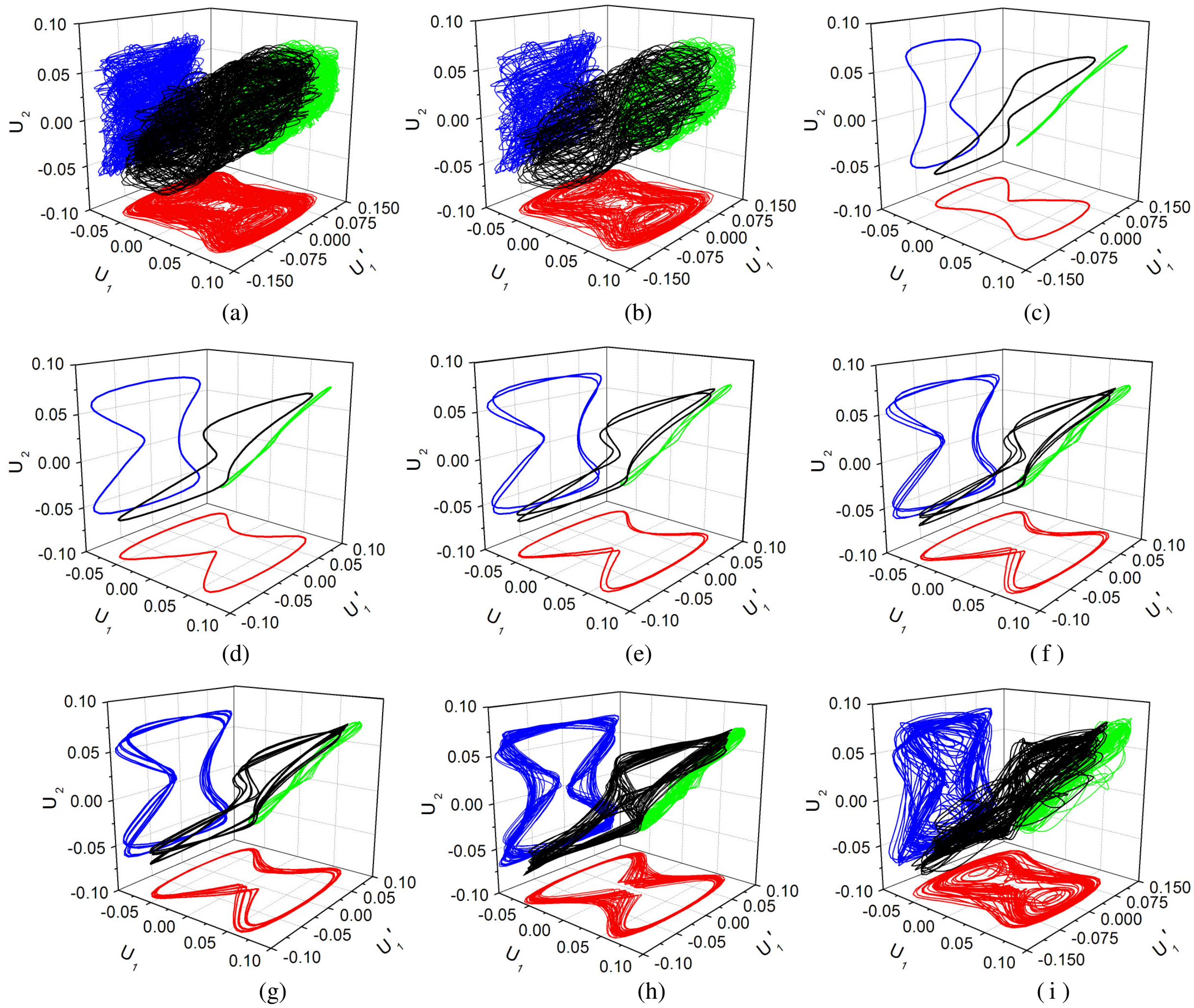

Figure 4. Trajectories on state subspaces U_1 x U_2 x U_1'.
(a) Hyperchaos ($\theta_2 = 1.44$); (b) Hyperchaos ($\theta_2 = 1.75$); (c) Period-1 ($\theta_2 = 1.804$);
(d) Period-1 ($\theta_2 = 2.10$); (e) Period-2 ($\theta_2 = 2.15$); (f) Period-4 ($\theta_2 = 2.20$);
(g) Period-8 ($\theta_2 = 2.28$); (h) Chaos ($\theta_2 = 2.34$); (i) Chaos ($\theta_2 = 2.44$).

In Figs. 4(a) and 4(b), a non-regular dynamical response is identified is the subspace. After taking the *Poincare* section for these two cases, Figs. 5(a) and 5(b) show tangled points without a defined structure. This lack of structure suggests hyperchaotic situations for both cases.

In Figs. 4(c) and 4(d), there is a closed orbit in the subspace, which characterizes a periodic behavior. Besides that, this closed orbit always follows a single path, indicating a period-1 behavior. It is worthwhile to remember that the result obtained for Fig. 4(c) concerns the value of $\theta_2 = 1.804$ that is placed within a periodic window immersed in a chaotic region, according to the first detail of each of the two Figs. 3(a) and 3(b). The *Poincare* sections for these two cases show a single point, attesting a periodic behavior of period-1.

In the subsequent Figs. 4(e), 4(f) and 4(g), there are still closed orbits in the subspace, indicating periodic behaviors; however, for these cases, the orbits follow multiple paths, according to the respective periodicity. The *Poincare* sections showed in Figs. 5(e), 5(f) and 5(g), for period-2, period-4 and period-8, respectively, ensure the periodic characteristic of each of these responses.

In Figs. 4(h) and 4(i), it is possible to observe a more regular dynamical response, while compared to Figs. 4(a) and 4(b). Taking the *Poincare* sections for these two cases (Figs. 5h and 5i), lamellar structures arise, characterizing strange attractors that, in turn, suggest a chaotic behavior.

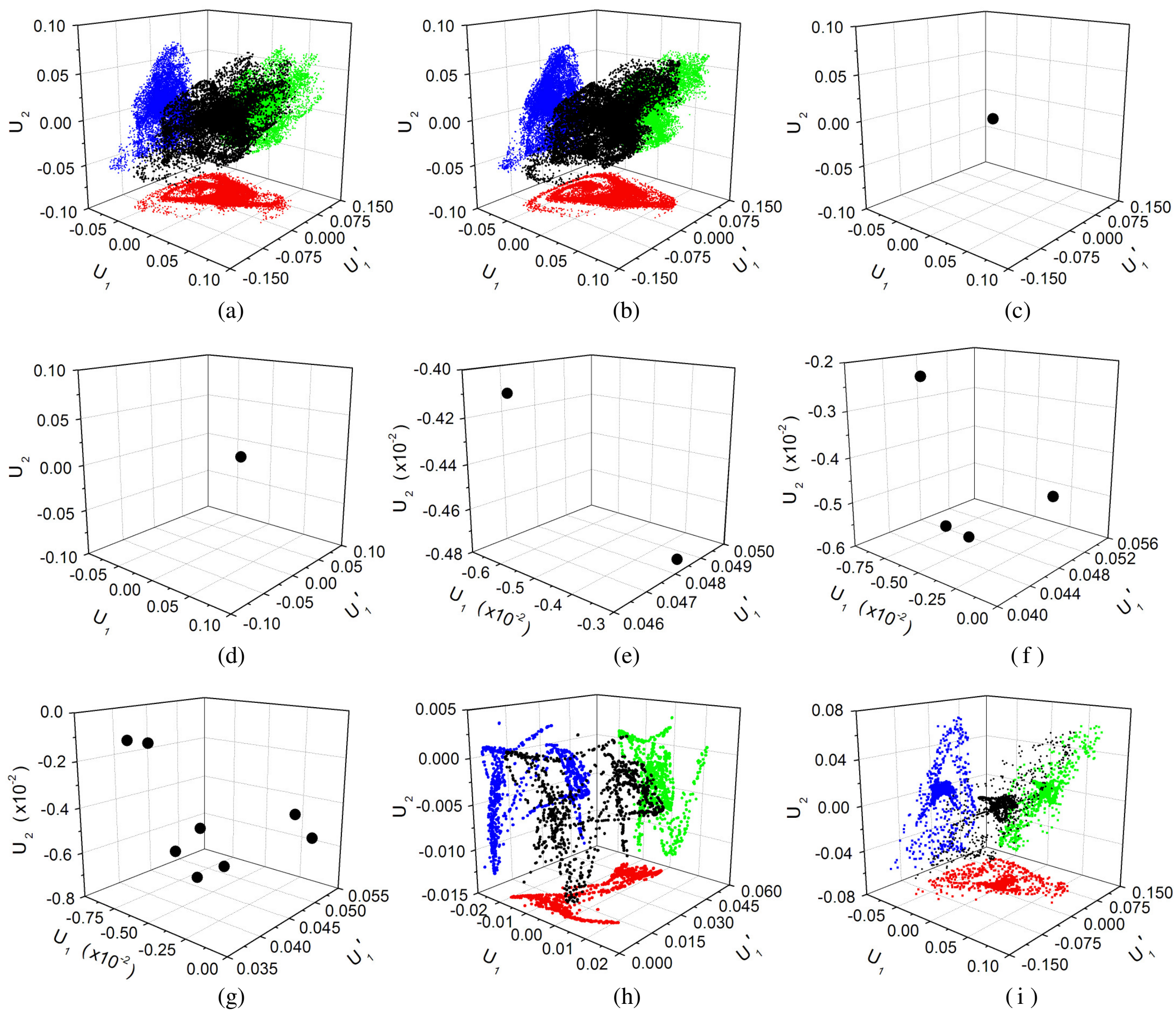

Figure 5. *Poincare* sections on state subspaces U_1 x U_2 x U_1'.
(a) Hyperchaos ($\theta_2 = 1.44$); (b) Hyperchaos ($\theta_2 = 1.75$); (c) Period-1 ($\theta_2 = 1.804$);
(d) Period-1 ($\theta_2 = 2.10$); (e) Period-2 ($\theta_2 = 2.15$); (f) Period-4 ($\theta_2 = 2.20$);
(g) Period-8 ($\theta_2 = 2.28$); (h) Chaos ($\theta_2 = 2.34$); (i) Chaos ($\theta_2 = 2.44$).

Figure 6 shows the *Lyapunov* spectra for six of the nine cases explored in Figs. 4 and 5.

Figs. 6(a) and 6(b) present two positive *Lyapunov* exponents, confirming that, for $\theta_2 = 1.44$ and $\theta_2 = 1.75$, the system has a hyperchaotic behavior.

In Figs. 6(c) and 6(d), all four *Lyapunov* exponents are negative, characterizing periodic behaviors for the period-1 response with $\theta_2 = 1.804$ and for period-8 response with $\theta_2 = 2.28$. The other three periodic cases (period-1 for $\theta_2 = 2.10$; period-2 for $\theta_2 = 2.15$ and period-4 for $\theta_2 = 2.20$) were verified and all them also present all *Lyapunov* exponents negative. For conciseness, the *Lyapunov* exponents for these cases were omitted.

In Figs. 6(e) and 6(f), there is only one positive *Lyapunov* exponent, which indicates that these two situations ($\theta_2 = 2.34$ and $\theta_2 = 2.44$) are associated to chaotic responses.

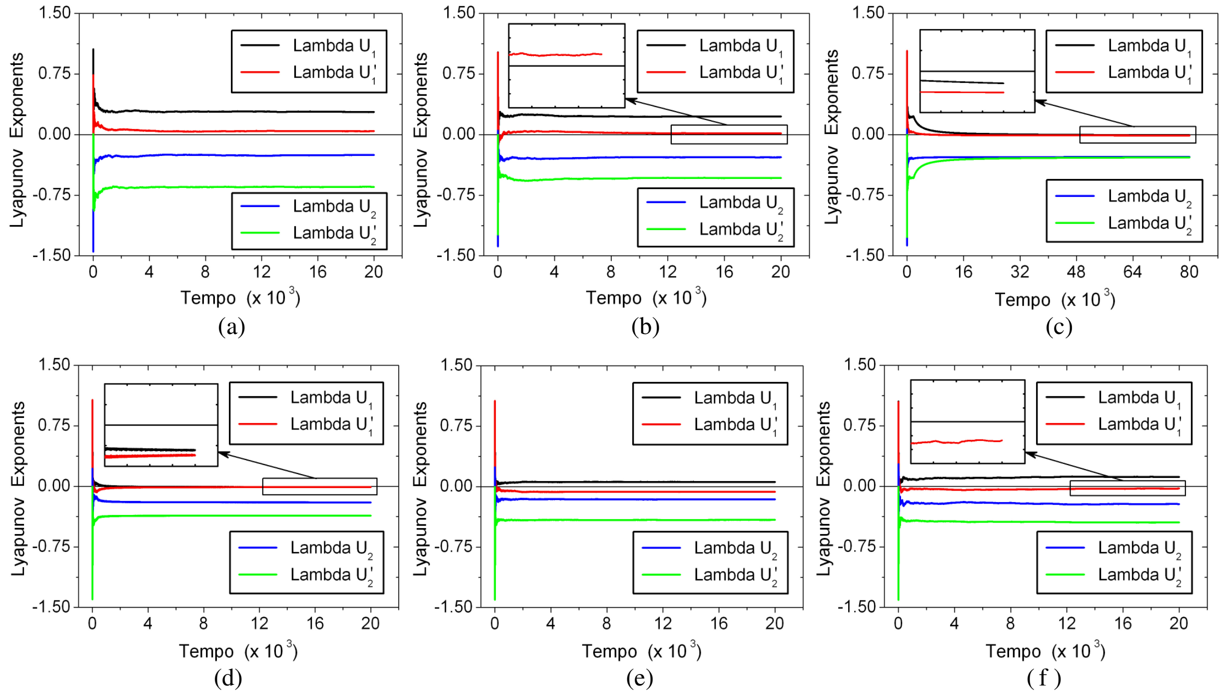

Figure 6. *Lyapunov* espectra for different temperatures of the intermediate **SMA** element.
(a) Hyperchaos ($\theta_2 = 1.44$); (b) Hyperchaos ($\theta_2 = 1.75$); (c) Period-1 ($\theta_2 = 1.804$);
(d) Period-8 ($\theta_2 = 2.28$); (e) Chaos ($\theta_2 = 2.34$); (f) Chaos ($\theta_2 = 2.44$).

Figure 7 shows the converged values for the *Lyapunov* spectra for each value of the dimensionless temperature θ_2, superposed to the bifurcation diagram for displacement U_1 varying as function of the temperature of the intermediate **SMA** element. The bifurcation diagram presented in next Fig. 7 is the same shown in Fig. 3(a).

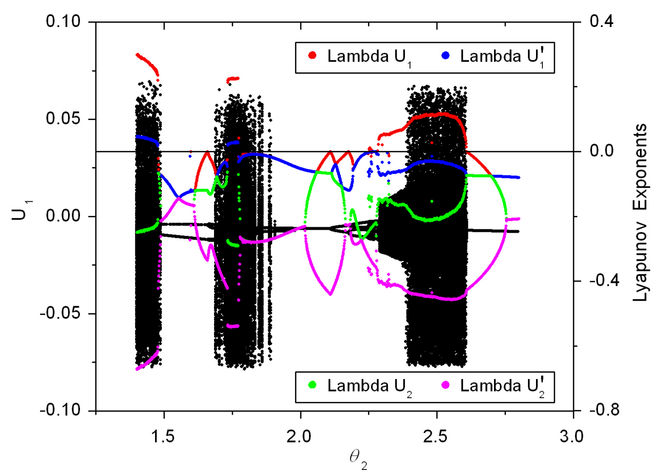

Figure 7. Converged values for *Lyapunov* spectra superposed to bifurcation diagram.

By the diagram of Fig. 7, it becomes clear that the first chaotic-like region is, actually all hyperchaotic, with two positive *Lyapunov* exponents (red and blue) within all this range. In the second chaotic-like region, only a short range (around θ_2 = 1.75) is hyperchaotic (red and blue positive exponents), being the rest of this region periodic with high periodicity (all four negative exponents), despite of the cloud of points. The third chaotic-like region is all chaotic, showing only one positive *Lyapunov* exponent (in red). All the information provided by this diagram is in perfect agreement with all previous results.

4. CONCLUDING REMARKS

This paper addresses the nonlinear analysis of a coupled two-degree of freedom oscillator with three **SMA** restoring elements, considering a polynomial constitutive formulation. A thorough dynamical investigation is conducted based on the variation of the temperature of the intermediate **SMA** element. Initially, a bifurcation diagram indicates different dynamical patterns, ranging from periodic to chaotic solutions, together with crisis and periodic windows. Then, periodic solutions with different periodicity and chaotic responses are illustrated through trajectories on state subspaces and *Poincare* sections. At last, the chaotic-like responses are differentiated by means of *Lyapunov* exponent analyses, into chaotic and hyperchaotic regions. All the results obtained for trajectories on state subspaces, *Poincare* sections and *Lyapunov* exponents are in agreement with the bifurcation diagram forecast.

5. ACKNOWLEDGEMENT

The authors would like to acknowledge the support of the Brazilian Research Agencies CNPq, CAPES, FAPERJ as well as INCT-EIE (National Institute of Science and Technology - Smart Structures in Engineering). The acknowledgement applies also to Air Force Office of Scientific Research (AFOSR).

6. REFERENCES

Bernardini, D. & Rega, G.; 2005; “Thermomechanical Modelling, Non-linear Dynamics and Chaos in Shape Memory Oscilators”; Mathematical and Computer Modelling of Dynamical Systems; Vol. 11; N. 3; pp. 291–314.

Birman, V.; 1997; “Review of Mechanics of Shape Memory Alloys Structures”; Applied Mechanics Review; Vol. 50; N. 11; pp. 629–645.

Duerig, T.; Melton, K.; Stöckel, D. & Wayman, C.; 1990; “Engineering Aspects of Shape Memory Alloys”; Ed. Butterworth-Heinemann; 499 pp.

Falk, F.; 1980; “Model Free-energy, Mechanics and Thermodynamics of Shape Memory Alloys”; ACTA Metallurgica; Vol. 28; pp. 1773–1780.

Lagoudas, D.C., Khan, M.M., Mayes, J.J. & Henderson, B.K.; 2004; “Pseudoelastic SMA Spring Elements for Passive Vibration Isolation: Part II - Simulations and Experimental Correlations”; Journal of Intelligent Material Systems and Structures; Vol. 15; N. 6; pp. 443–470.

Lagoudas, D.C.; 2008; “Shape Memory Alloys – Modeling and Engineering Applications”; Ed. Springer; 435 pp.

Machado, L.G.; Savi, M.A. & Pacheco, P.M.L.C.; 2003; “Nonlinear Dynamics and Chaos in Coupled Shape Memory Oscillators”; International Journal of Solids and Structures; Vol. 40; N. 19; pp. 5139–5156.

Machado, L.G.; Savi, M.A. & Pacheco, P.M.L.C.; 2004; “Bifurcations and Crises in a Shape Memory Oscillator”; Shock and Vibration; Vol.11; N. 2; pp. 67–80.

Otsuka, K. & Wayman, C.M.; 1998; “Shape Memory Materials”; Ed. Cambridge Univ. Press; 284 pp.

Paiva, A. & Savi, M.A.; 2006; “An Overview of Constitutive Models for Shape Memory Alloys”; Mathematical Problems in Engineering; Vol. 2006, Article ID 56876, 30 pp.

Santos, B.C. & Savi, M.A.; 2009; “Nonlinear Dynamics of a Nonsmooth Shape Memory Alloy Oscillator”; Chaos, Solitons and Fractals; Vol. 40; pp. 197–209.

Savi, M.A. & Pacheco, P.M.L.C.; 2002; “Chaos and Hyperchaos in Shape Memory Systems”; International Journal of Bifurcation and Chaos; Vol. 12; N. 3; pp. 645–657.

Savi, M.A.; Sá, M.A.N.; Paiva, A. & Pacheco, P.M.C.L.; 2008; “Tensile-compressive Asymmetry Influence on Shape Memory Alloy System Dynamics”; Chaos, Solitons and Fractals; Vol. 36; pp. 828–842.

Savi, M.A.; De Paula, A.S. & Lagoudas, D.C.; 2011; “Numerical Investigation of an Adaptive Vibration Absorber Using Shape Memory Alloys” Journal of Intelligent Material Systems and Structures; Vol. 22; pp. 67–80.

Seelecke, S.; 2002; “Modeling the Dynamic Behavior of Shape Memory Alloys”; International Journal of Nonlinear Mechanics; Vol. 37; N. 8; pp. 1363–1374.

Silva, L.C.; Savi, M.A. & Paiva, A.; 2013; “Nonlinear Dynamics of a Rotordynamic Nonsmooth Shape Memory Alloy System”; Journal of Sound and Vibration; Vol. 332; pp. 608–621.

Wayman, C.M.; 1980; “Some Applications of Shape-Memory Alloys”; Journal of the Minerals, Metals & Materials Society; Vol. 32; N 6; pp 129–137.

Williams, K., Chiu, G. & Bernhard, R.; 2002; “Adaptive-passive Absorbers Using Shape-memory Alloys”; Journal of Sound and Vibration; Vol. 249; N. 5; pp. 835–848.

7. RESPONSIBILITY NOTICE

The authors are the only responsible for the printed material included in this paper.